ⓐ Open Access Full Text Article

ORIGINAL RESEARCH

Bufalin-loaded mPEG-PLGA-PLL-cRGD nanoparticles: preparation, cellular uptake, tissue distribution, and anticancer activity

Peihao Yin[1]*
Yan Wang[1]*
YanYan Qiu[1]
LiLi Hou[1]
Xuan Liu[1]
Jianmin Qin[1]
Yourong Duan[2]
Peifeng Liu[2]
Ming Qiu[3]
Qi Li[1]

[1]Department of Clinical Oncology, Putuo Hospital and Interventional Cancer Institute of Integrative Medicine, Shanghai University of Traditional Chinese Medicine, Shanghai, China; [2]Shanghai Cancer Institute, Jiaotong University, Shanghai, China; [3]Department of General Surgery, Changzheng Hospital, Second Military Medical University, Shanghai, China

*These authors contributed equally to this work

Correspondence: Qi Li
Dept of Clinical Oncology, Putuo Hospital & Interventional Cancer Institute of Integrative Medicine, Shanghai University of Traditional Chinese Medicine, Shanghai 200062, China
Tel +86 21 52669731
Fax +86 21 52665957
Email lzwf@hotmail.com

Ming Qiu
Department of General Surgery, Changzheng Hospital, Second Military Medical University, Shanghai, China
Tel +86 21 63610109 73944
Fax +86 21 63520020
Email qium127@sina.com

Background: Recent studies have shown that bufalin has a good antitumor effect but has high toxicity, poor water solubility, a short half-life, a narrow therapeutic window, and a toxic dose that is close to the therapeutic dose, which all limit its clinical application. This study aimed to determine the targeting efficacy of nanoparticles (NPs) made of methoxy polyethylene glycol (mPEG), polylactic-co-glycolic acid (PLGA), poly-L-lysine (PLL), and cyclic arginine-glycine-aspartic acid (cRGD) loaded with bufalin, ie, bufalin-loaded mPEG-PLGA-PLL-cRGD nanoparticles (BNPs), in SW620 colon cancer-bearing mice.

Methods: BNPs showed uniform size. The size, shape, zeta potential, drug loading, encapsulation efficiency, and release of these nanoparticles were studied in vitro. The tumor targeting, cellular uptake, and growth-inhibitory effect of BNPs in vivo were tested.

Results: BNPs were of uniform size with an average particle size of 164 ± 84 nm and zeta potential of 2.77 mV. The encapsulation efficiency was $81.7\% \pm 0.89\%$, and the drug load was $3.92\% \pm 0.16\%$. The results of in vitro cytotoxicity studies showed that although the blank NPs were nontoxic, they enhanced the cytotoxicity of bufalin in BNPs. Drug release experiments showed that the release of the drug was prolonged and sustained. The results of confocal laser scanning microscopy indicated that BNPs could effectively bind to human umbilical vein endothelial cells. In the SW620 xenograft mice model, the BNPs could effectively target the tumor in vivo. The BNPs were significantly more effective than other NPs in preventing tumor growth.

Conclusion: BNPs had even size distribution, were stable, and had a slow-releasing and tumor-targeting effect. BNPs significantly inhibited colon cancer growth in vitro and in vivo. As a novel drug carrier system, BNPs are a potentially promising targeting treatment for colon cancer.

Keywords: colon cancer, nanoparticles, tumor target, bufalin

Introduction

Colon cancer is a commonly occurring malignant tumor. Over recent years, the incidence of colon cancer has been gradually increasing;[1,2] therefore, the treatment of colon cancer has become a focus of research worldwide.

Bufalin is a major bioactive component of venenum bufonis, a traditional Chinese medicine obtained from the skin and parotid venom glands of toads.[3–5] Bufalin shows significant activity against a broad spectrum of tumors, including hematoma,[6,7] leukemia,[8,9] gastric cancer,[10] prostate cancer,[11] and ovarian cancer.[12] It was recently shown to be effective in inducing autophagy-mediated cell death in human colon cancer cells.[13] It can induce differentiation and apoptosis in cancer cells. Bufalin shows this activity against colon cancer cells through a reactive oxygen species-dependent

autophagy pathway.[14] However, it has adverse effects, such as high cardiac toxicity[15] and sudden death,[16,17] which limit its clinical application. To decrease the toxicity, the content of bufalin must be strictly controlled.[18] In addition, low water solubility[16] is also a shortcoming for intravenous preparation. There are also many clinical side effects, such as vaso-irritation, allergic shock, ardent fever, and sinus bradycardia, as a result of bufalin's wide distribution. The current preparation of venenum bufonis for tumor therapy is by Huachansu injection, a mixture of alkaloids found in venenum bufonis, which is available in market. There is, however, little bufalin in the Huachansu injection because of its low water solubility. Therefore, problems with this substance include poor targeting of the tumor and low concentration in the tumor.

Owing to improvements in the current encapsulation techniques, this limitation may be overcome by encapsulating bufalin in nanoparticle drug delivery systems (NPs). NPs can precisely deliver anticancer drugs to a tumor site, thereby reducing drug toxicity to normal tissues. NPs can be delivered to a tumor by passive or active mechanisms. Biodistribution of drug-loaded NPs is mainly related to the inherent properties of carriers, such as composition, size, and surface property. Studies suggest NPs with sizes of 0.1–5 nm can be eliminated from the blood quickly. NPs less than 50 nm can reach the spleen and marrow through the endothelium of the liver or pass through the lymphatic system. NPs with diameters less than 200 nm can permeate into the tumor microvasculature.[19] Thus, the size of NPs should be controlled with respect to the targeted organs.

Some NPs of bufalin are currently being studied to enhance the antitumor efficiency and decrease side effects. Bufadienolide (consisting of bufalin, binobufagin, and resibufogenin) liposomes prolonged the retention time and increased the area under the curve in vivo, causing no allergen-related or blood vessel irritation effects.[20] The lipid microsphere also exhibited a longer half-life time.[21] The results of nanostructured lipid particles were similar and showed that the chemical stability of bufalin was enhanced by being encapsulated in lipid particles.[22] The merits of these NPs were based on the sustained-release of the drug from the NPs.

Targeted delivery carriers that can concentrate the drug within the tumor and reduce its toxic side effects on normal tissues have become the focus of research worldwide. A targeted moiety conjugated onto the surface of NPs can ensure their delivery to the target site by receptor-mediated recognition.[23,24] Integrin $\alpha_v\beta_3$ is overexpressed on the endothelial cells of vascularization, which is responsible for tumor growth; conversely, $\alpha_v\beta_3$ integrin is not expressed on normal tissues. $\alpha_v\beta_3$ integrin is an ideal target molecule.[25,26]

Because arginine-glycine-aspartic acid (RGD) can effectively bind to $\alpha_v\beta_3$,[27,28] it serves as the basis for the active targeting of NPs. In this experiment, we used methoxy polyethylene glycol (mPEG), polylactic-co-glycolic acid (PLGA), poly-L-lysine (PLL), and cyclic RGD (cRGD) to prepare mPEG-PLGA-PLL-cRGD as the carrier and bufalin as the model drug to prepare bufalin-mPEG-PLGA-PLL-cRGD NPs. PLGA and PLL have good biodegradability and biocompatibility and can achieve a sustained-release effect by gradually degrading in vivo.[29–32] A water-soluble mPEG block produces NPs with good biocompatibility and long circulation properties that enhance the targeting ability of NPs;[33,34] in addition, it can increase the amount of residual NPs in the tumor through the enhanced permeability and retention (EPR) effect.[35] In order to verify these properties of the NPs, various properties of bufalin-mPEG-PLGA-PLL-cRGD NPs were studied in detail.

Methods
Materials
Bufalin was purchased from Chengdu PuRuiFa Technology Development Co. Ltd (Chengdu, China); human umbilical vein endothelial cells (HUVECs), SW620 colon cancer cells, and BALB/c female athymic nude mice from the Shanghai Cancer Institute (Shanghai, China); 4', 6-diamidino-2-phenylindole (DAPI) from Shanghai Future Biological Technology Co, Ltd (Shanghai, China); rhodamine B (Rb) from Sigma-Aldrich (St Louis, MO); and the WST-8 Cell Proliferation Assay Kit from Cayman Chemical (Ann Arbor, MI). mPEG-PLGA-PLL-cRGD (MW 11,000; mPEG-PLGA-PLL:RGD = 1:1) was synthesized using a previously described method.[16] We used the following instruments: JY92-II ultrasonic processor (Ningbo Scientz Biotechnology Co, Ltd, Ningbo, China), confocal laser scanning microscope (CLSM) (FV1000; Olympus, Tokyo, Japan), Nicomp 380/ZLS zeta potential analyzer (Particle Sizing System, USA), TU-1901 ultraviolet–visible spectrophotometer (Beijing Purkinje General Co, Ltd, Beijing, China), transmission electron microscope (TEM) (JEM-100SX; Japan Electron Company, Tokyo, Japan), and small animal in vivo fluorescence imaging system (LB 983; Berthold Technologies Gmbh and Co KG, Bad Wildbad, Germany).

Preparation of bufalin-mPEG-PLGA-PLL-cRGD NPs
Bufalin-mPEG-PLGA-PLL-cRGD NPs were prepared as described previously.[36] Briefly, 4 mg mPEG-PLGA-PLL-cRGD polymers was dissolved in 200 μL methylene dichloride solution of bufalin (1 mg/mL). The solution was poured into a 2.2 mL aqueous solution of Pluronic F-68 (1% weight/volume;

Sigma-Aldrich), and emulsified using an ultrasonic processor for 1 minute (10 seconds × 4). Subsequently the emulsion was stirred at room temperature for 2 hours then evacuated to remove the organic phase. The solution was centrifuged (8000 rpm × 5 minutes) to remove sediment.

For a comparative study, we replaced mPEG-PLGA-PLL-cRGD with mPEG-PLGA-PLL and prepared bufalin-mPEG-PLGA-PLL NPs using the previously mentioned methods.

Characterization of bufalin-mPEG-PLGA-PLL-cRGD NPs

The mean particle size and zeta potential of the bufalin-mPEG-PLGA-PLL-cRGD NPs at 25°C was determined by using the Nicomp 380/ZLS zeta potential analyzer. Morphological evaluation of the bufalin-mPEG-PLGA-PLL-cRGD NPs was performed by using TEM. The entrapment efficiency of bufalin in the NPs was determined after ultracentrifugation. Briefly, 5 mL of the NPs was subjected to ultrafiltration (molecular weight cutoff, 10 kDa) and centrifuged at 14,000 rpm for 20 minutes. The solution in the lower chamber obtained during the centrifugation was assayed spectrometrically at 298 nm by using the TU 1901 ultraviolet (UV)-visible spectrophotometer to get the free bufalin. The encapsulated bufalin was calculated with the total amount subtracted by the free amount. The encapsulation efficiency was expressed as the percentage of bufalin encapsulated in the NPs versus the total amount of bufalin used initially. The drug-loading amount was expressed as the percentage of bufalin encapsulated in the NPs versus the total amount of NPs used initially. The encapsulation efficiency and drug-loading rates were represented by the following equations:

Encapsulation efficiency = the amount of bufalin encapsulated in NPs/the amount of bufalin in NP solution × 100%

Drug-loading amount = the amount of bufalin encapsulated in NPs/the total amount of NPs × 100%

Each suspension sample was diluted to the appropriate concentration with filtered distilled water and kept for 4 minutes to obtain a steady state. Each sample was analyzed in triplicate.

Drug release in vitro

The saturate solubility of bufalin was 32.76 μg/mL in pH 7.0 and 29.86 μg/mL in pH 7.8–8.0.[37] The volume of medium was three times the saturated solution of bufalin. For comparing the sustained-release properties of free bufalin, bufalin-mPEG-PLGA-PLL NPs, and bufalin-mPEG-PLGA-PLL-cRGD NPs,

a dialysis tube (molecular weight cut-off [MWCO], Consumer & Industrial Specialties, 7 kDa) containing 2 mL of NP solution was directly immersed into 18 mL of phosphate-buffered saline (PBS, pH = 7.4) at 37°C and subjected to horizontal shaking (120 rpm/minute). Aliquots of 2 mL were drawn from the solution at predetermined intervals and replaced with 2 mL fresh PBS. The amount of bufalin in the samples at each time point was determined using a UV-visible spectrophotometer at 298 nm and calibrated to draw the release curves, using the following formula:

$$C_{0\,Cal} = C_0,$$
$$C_{i+1\,Cal} = C_{i+1} + V_{sample} * C_{i\,Cal}/V_{total},$$

where i is from from 0 to n, C_{Cal} is the calibrated concentration, C is the determined concentration, V_{sample} is the volume of aliquots taken out of the medium, and V_{total} is the volume of the total medium.

Pharmacokinetics

In pharmacokinetics, mice bearing hepatoma were randomly divided into two groups. Bufalin (1 mg/kg) and bufalin-loaded mPEG-PLGA-PLL-cRGD nanoparticles (BNPs) (containing bufalin 1 mg/kg) were administered to each group through the caudal vein. At predetermined time points (5, 15, 30, and 45 minutes and 1, 2, 4, 6, 12, and 24 hours) of post-intravenous (iv) dose, blood was collected from the caudal vein. At predetermined time points post injection, six mice from each group at each time point were euthanized by cervical dislocation and dissected. Plasma was collected at 2 hours post-iv dose. Plasma samples were frozen at −20°C until analysis. The bufalin content in pharmacokinetics was analyzed by high performance liquid chromatography.

Plasma pharmacokinetic parameters were assessed by the compartmental technique with the software program DAS (version 2.0; Debris Assessment Software, Houston, TX). The area under the curve of concentration versus time (AUC) from zero to the last time point was calculated by the log-linear trapezoidal method.

Cell culture

SW620 colon cancer cells and HUVECs were cultured in Dulbecco's Modified Eagle's Medium (DMEM; GIBCO, New York, NY) supplemented with 10% fetal bovine serum (Minhai, Gansu, China) at 37°C under a humidified environment of 5% CO_2.

In vitro growth-inhibitory effect of NPs

The cytotoxic effect of the NPs on SW620 colon cancer cells was evaluated by using the cholecystokinin (CCK)-8 assay.

Briefly, SW620 colon cancer cells were seeded in 96-well plates at a density of 5×10^4 cells/well and incubated (37°C, 5% CO_2) for 24 hours. Different amounts of free bufalin, bufalin-mPEG-PLGA-PLL NPs, and bufalin-mPEG-PLGA-PLL-cRGD NPs were added into these wells to make final concentrations of 0.5, 1, 2, 4, 6, and 8 nM; the cells were then incubated for 24 hours. Subsequently, 10 μL of CCK-8 assay agents were added to the culture medium, and the cells were incubated for 1 hour. Absorbance was measured at 450 nm.

Cellular uptake of NPs

Rb (418 nM) instead of bufalin was encapsulated in mPEG-PLGA-PLL and mPEG-PLGA-PLL-cRGD NPs as a fluorescence probe for studying the uptake of these molecules. DAPI was used as a nucleus marker. For CSLM examination, SW620 colon cancer cells and HUVECs were seeded in a glass-bottom dish (MatTek Corporation, Ashland, MA) at a density of 4×10^6 and incubated for 24 hours. Rb-mPEG-PLGA-PLL and Rb-mPEG-PLGA-PLL-cRGD NPs (200 μL) were added to these cells and incubated for 2 hours at 37°C; then, the cells were incubated with DAPI for 10 minutes and washed thrice with PBS. The NPs were visualized under a CLSM.

Establishment of a tumor model

Subcutaneous tumors were established in 4- to 6-week-old, BALB/c, female, athymic, nude mice by injecting 5×10^6 SW620 cells into their dorsal subcutaneous space. After establishing the tumor model, the tumor-bearing mice were classified into two groups (n = 10): (a) Rb-mPEG-PLGA-PLL and (b) Rb-mPEG-PLGA-PLL-cRGD.

Tumor targeting

The animal study protocols were approved by the Animal Study Committee of Shanghai Cancer Institute. To study the target effect of mPEG-PLGA-PLL-cRGD NPs in SW620 colon cancer xenograft tumors in vivo, Rb (418 nM) instead of bufalin was encapsulated as a fluorescence probe in mPEG-PLGA-PLL and mPEG-PLGA-PLL-cRGD NPs. Rb-mPEG-PLGA-PLL and Rb-mPEG-PLGA-PLL-cRGD NPs (20 μL) were injected through the vena caudalis (tail vein) into the tumor-bearing SW620 xenografted mice. Fluorescence imaging of the tumor-bearing mice was performed at 4 and 32 hours after injection by using a small animal in vivo fluorescence imaging system.

In vivo study of the therapeutic efficacy in mice

The mice were classified into six groups on the basis of the solutions they were administered: normal saline group (NS, 13.5 mL/kg), mPEG-PLGA-PLL NP group (mPEG-PLGA-PLL NPs, 24.5 mg/kg), bufalin solution group (bufalin, 1 mg/kg), mPEG-PLGA-PLL-cRGD NP group (mPEG-PLGA-PLL-cRGD NPs 24.5 mg/kg), bufalin-mPEG-PLGA-PLL NP group (bufalin-mPEG-PLGA-PLL, 1 mg/kg), and bufalin-mPEG-PLGA-PLL-cRGD NP group (bufalin-mPEG-PLGA-PLL-cRGD, 1 mg/kg), by injection through the vena caudalis once a day.

The remaining mice in each group were killed and the tumors were removed for examination. The longest (a) and the longest (b) vertical dimensions of the tumor were measured. The size (V) of the tumor was calculated using the following equation:

$$V = ab^2/2$$

Results
Characterization of bufalin-mPEG-PLGA-PLL-cRGD NPs

Morphology, size distribution, and zeta potential of the BNPs is show in Figure 1. The mPEG-PLGA-PLL-cRGD NPs were spherical and well-dispersed particles (Figure 1A). The size distribution of the mPEG-PLGA-PLL-cRGD NPs was almost homologous, with a diameter of 164 ± 84 nm (polydispersity index [PDI] = 0.209) (Figure 1B), and their zeta potential was 2.77 mV (Figure 1C). The particle size of NPs affects their endocytosis by tumor cells and has a great influence on the in vivo distribution of the NPs. Generally, the NPs (size < 200 nm) may deposit more in solid tumors via EPR because of PEG in the outer layer, so the mPEG-PLGA-PLL-cRGD NPs was expected to show good passive targeting to the tumor.

The UV determination wavelength was 298 nm (Figure 2), but the polymers have no absorption at this wavelength. The encapsulation efficiency and drug-loading amount of the bufalin-mPEG-PLGA-PLL-cRGD NPs was $81.7\% \pm 0.89\%$ and $3.92\% \pm 0.16\%$, respectively (Table 1, n = 3). The preparation method was shown to be repeatable.

Drug release in vitro

The in vitro cumulative drug-release profile is shown in Figure 3. Over time, bufalin in NPs was released much more slowly than free drug. At 24 hours, the cumulative bufalin release in free drug was about 90% but about 50% in NPs. The 90% cumulative release in NPs came at 192 hours, suggesting that in comparison with the free drug, bufalin-mPEG-PLGA-PLL and bufalin-mPEG-PLGA-PLL-cRGD NPs have sustained-release properties. However, there was no obvious difference between the two NPs in the release profile.
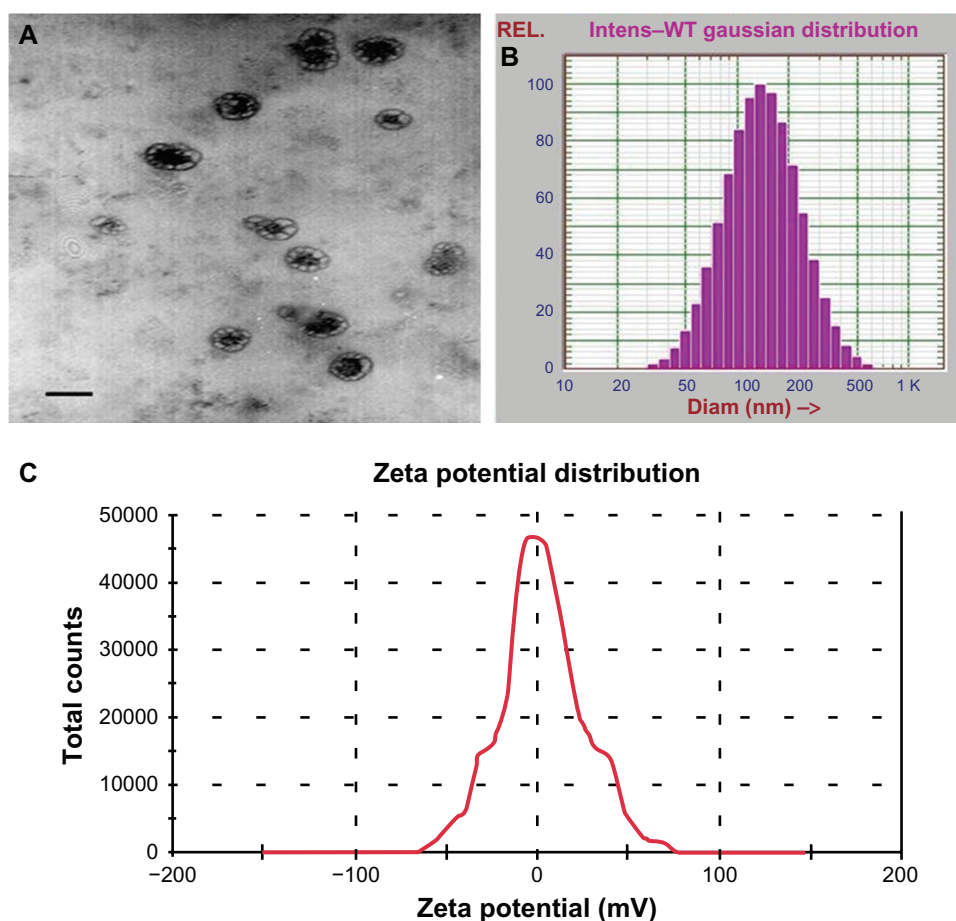
Figure 1 TEM (**A**), size distribution (**B**), and zeta potential (**C**) images of bufalin-mPEG-PLGA-PLL-cRGD NPs.
Abbreviations: NPs, nanoparticle drug delivery systems; TEM, transmission electron microscopy.

PLGA-PLL, which is the main component of the polymers used in this experiment, is a biodegradable material. Because of the poor water solubility of bufalin, it is hard for it to permeate through the matrix of the NP. The sustained release of the drug might mainly contribute to the degradation rates of the NPs prepared with these polymers. Therefore, the results showed that the NPs have a good sustained-release function. In clinical use, slow release of a drug may help achieve a stable drug concentration in vivo, thus giving a persistent and curative effect and avoiding the side effects related to drug concentration. In addition, mPEG conjugated to the mPEG-PLGA-PLL-cRGD could enable the NPs to evade phagocytosis by the reticuloendothelial system. PEG can also lead to more deposition on solid tumors through enhanced permeability and retention. This property not only improves the targeting efficacy of NPs but also enhances their slow-release effect for it provides an aqueous membrane outside of the NPs to hold back the release of a lipophilic drug.[38]

Figure 2 UV spectrum of PBS, mPEG-PLGA-PLL-cRGD and bufalin.
Abbreviation: PBS, phosphate-buffered saline.

Table 1 Encapsulation efficiency and drug-loading rate of bufalin-mPEG-PLGA-PLL-cRGD NPs

No	Encapsulation efficiency (%)	Drug-loading rate (%)
1	82.67	4.09
2	81.52	3.78
3	80.91	3.89

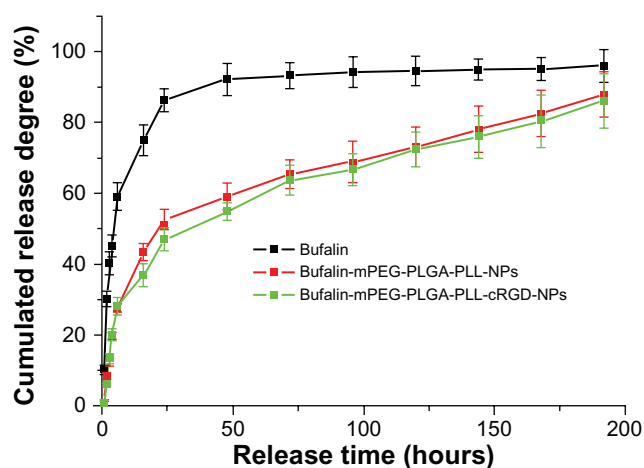**Abbreviation:** NPs, nanoparticle drug delivery systems.

Figure 3 Drug-release profile of NPs.
Abbreviation: NPs, nanoparticle drug delivery systems.

Pharmacokinetics and tissue distribution

The results of the pharmacokinetic studies are shown in Table 2. The concentration of free bufalin in plasma declined bi-exponentially and was significantly higher than BNPs ($P < 0.05$) at all time points. In plasma, bufalin was detectable even 24 hours after injection in BNP-treated animals, while bufalin was not detected in the plasma of animals treated with free bufalin. The plasma AUC and elimination half-life of BNPs were significantly greater than that of free bufalin. The mean residence time was prolonged from 3.45 hours to 7.63 hours; the apparent volume of distribution was increased and the clearance of bufalin was slower with BNPs compared to that of free bufalin in mice.

In vitro growth-inhibitory effect of NPs

The cRGD-modified mPEG-PLGA-PLL NPs could target tumor cells and inhibit angiogenesis and proliferation of tumor blood vessels. Additionally, bufalin could directly

Table 2 The main pharmacokinetic parameters of compartment model estimation

Parameter	Bufalin	BNPs
$AUC_{(0-t)}$ (mg/L*h)	0.26 ± 0.02	0.11 ± 0.01
$AUC_{(0-\infty)}$ (mg/L*h)	0.57 ± 0.02	0.43 ± 0.06
$MRT_{(0-t)}$ (h)	1.31 ± 0.11	2.32 ± 0.28
$MRT_{(0-\infty)}$ (h)	3.45 ± 0.37	7.63 ± 0.85
$t_{1/2z}$ (h)	3.35 ± 0.31	7.17 ± 2.05
T_{max} (h)	0.083 ± 0.011	0.083 ± 0.009
V_z (L/kg)	63.37 ± 1.56	187.83 ± 2.48
C_{max} (mg/L)	0.61 ± 0.040	0.34 ± 0.011

Note: Values are mean ± standard deviation (n = 3).
Abbreviations: AUC, area under the curve; MRT, mean residence time; $t_{1/2z}$, elimination half-life; T_{max}, time of maximum concentration; V_z, apparent volume of distribution; C_{max}, maximal concentration; BNPs, bufalin-loaded mPEG-PLGA-PLL-cRGD nanoparticles.
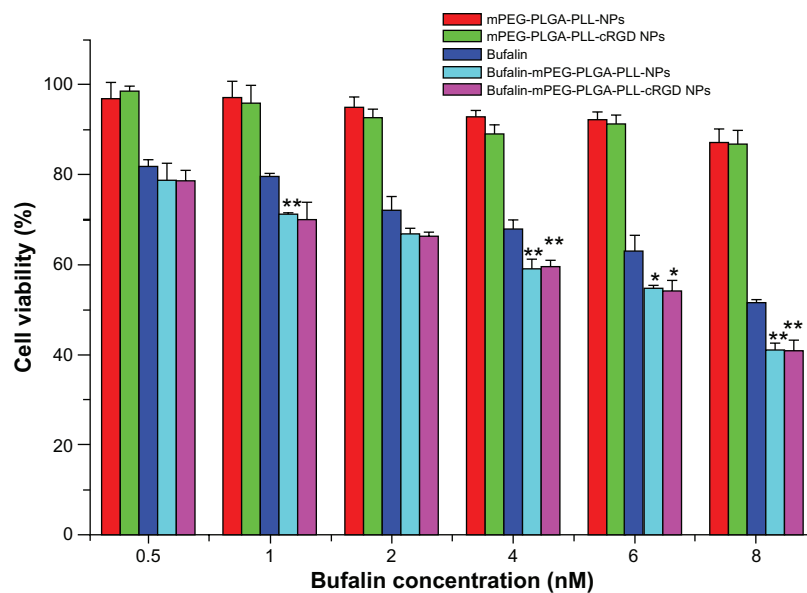
kill the SW620 colon cancer cells.[13] Therefore, we chose it as model cell to study the polymers and drug-loaded NPs for their growth-inhibitory effects.

The in vitro growth inhibitory effect of NPs on the SW620 colon cancer cells was evaluated using the CCK-8 assay. The SW620 colon cancer cells treated with increasing doses of mPEG-PLGA-PLL and mPEG-PLGA-PLL-cRGD blank NPs showed 90% to 96% viability, respectively. This finding suggests that the blank NPs were nontoxic at each of the tested concentrations (Figure 4).

Figure 4 also shows that the growth-inhibitory effect of bufalin-mPEG-PLGA-PLL and bufalin-mPEG-PLGA-PLL-cRGD NPs on SW620 colon cancer cell was significantly higher (by *t* test) than that of free bufalin when bufalin concentration was ≥4 nM. These results suggest that bufalin-loaded NPs could improve the growth inhibitory effect. However, the growth inhibitory effect of the two NPs was similar ($P > 0.05$). A possible reason for this is that there was efficient uptake of NPs by cells through endocytosis, while there is no $\alpha_v\beta_3$ integrin expression on SW620 cells so cRGD did not show further advised effect. To evaluate the target of cRGD to $\alpha_v\beta_3$ integrin, we carried out a cell uptake study.

Cellular uptake study

The therapeutic effect of a drug is closely associated with the amount of drug taken up by the cells. Therefore, the evaluation of NP uptake is important. We chose SW620 colon cancer cells, which have no $\alpha_v\beta_3$ integrin expression, and HUVECs, which have $\alpha_v\beta_3$ integrin expression on the cell membrane, to study cellular uptake.

As shown in Figure 5A and B, the Rb fluorescence intensity of the cells incubated with Rb-mPEG-PLGA-PLL and Rb-mPEG-PLGA-PLL-cRGD NPs was not significantly different. The main reason for this was that the surface of SW620 cells did not express $\alpha_v\beta_3$ integrins, thus the Rb-mPEG-PLGA-PLL and Rb-mPEG-PLGA-PLL-cRGD NPs were mainly internalized in the cells via the same model – endocytosis or phagocytosis.

As shown in Figure 5 C and D, the Rb fluorescence intensity of the cells incubated with Rb-mPEG-PLGA-PLL-cRGD NPs (C) was significantly higher than that of the cells incubated with Rb-mPEG-PLGA-PLL NPs (D). This finding shows that the cellular uptake of Rb-mPEG-PLGA-PLL-cRGD NPs by HUVEC is more effective than that of Rb-mPEG-PLGA-PLL NPs. The main reason was that Rb-mPEG-PLGA-PLL-cRGD NPs could be internalized in the cells via their ability to preferentially bind with $\alpha_v\beta_3$ integrins, which were overexpressed on HUVECs. The present experimental results

Figure 4 Cellular viability of SW620 colon cancer cells after 24 hours culture with free bufalin and bufalin-NPs.
Notes: *$P < 0.05$ when compared with bufalin; **$P < 0.01$ when compared with bufalin by *t*-test.
Abbreviation: NPs, nanoparticle drug delivery systems.

further showed that, compared to the Rb-mPEG-PLGA-PLL NPs, Rb-mPEG-PLGA-PLL-cRGD NPs have ideal $\alpha_v\beta_3$ integrin-targeting properties and better therapeutic potential.

Tumor targeting of NPs

Rb-mPEG-PLGA-PLL and Rb-mPEG-PLGA-PLL-cRGD NPs were used to investigate its tumor-targeting efficiency in vivo. Figure 6 shows the results of the targeted imaging.

At 4 hours post injection, the tumor fluorescence intensity of the mice treated with Rb-mPEG-PLGA-PLL NPs and that of mice treated with Rb-mPEG-PLGA-PLL-cRGD NPs showed no significant difference. After 32 hours postinjection, the tumor fluorescence intensity of mice injected with Rb-mPEG-PLGA-PLL NPs gradually decreased. However, the tumor fluorescence intensity of mice injected with Rb-mPEG-PLGA-PLL-cRGD NPs was relatively stronger and lasted
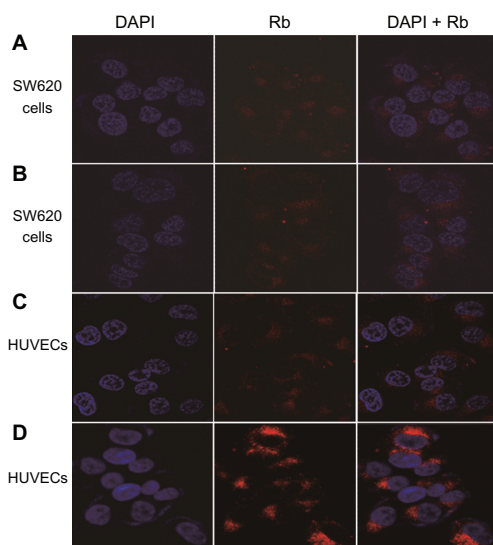
Figure 5 Confocal images of SW620 colon cancer cells and HUVECs after treatment with Rb-mPEG-PLGA-PLL NPs (**A**) and Rb-mPEG-PLGA-PLL-cRGD NPs (**B**), and confocal images of HUVECs after treatment with Rb-mPEG-PLGA-PLL NPs (**C**) and Rb-mPEG-PLGA-PLL-cRGD NPs (**D**).
Abbreviations: HUVECs, human umbilical vein endothelial cells; NPs, nanoparticle drug delivery systems; Rb, rhodamine B.
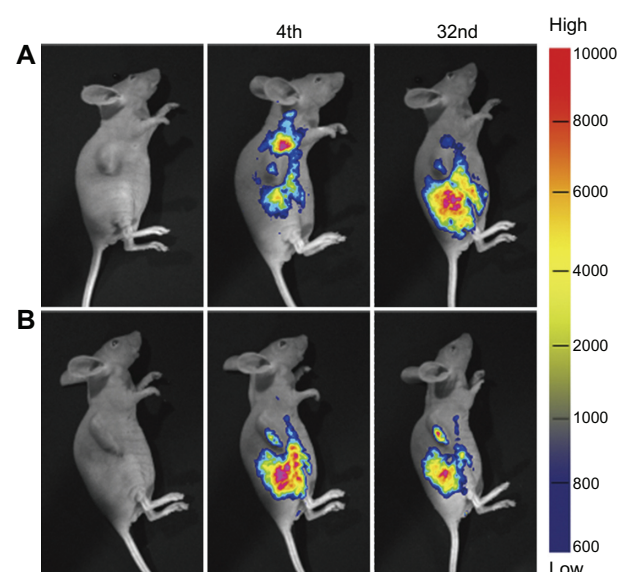

Figure 6 In vivo noninvasive targeted imaging of the tumor-bearing mice injected with Rb-mPEG-PLGA-PLL (**A**) and Rb-mPEG-PLGA-PLL-cRGD (**B**) NPs.
Notes: The colors indicate the changes in fluorescence signal intensity from high (red) to low (blue).
Abbreviations: NPs, nanoparticle drug delivery systems; Rb, rhodamine B.
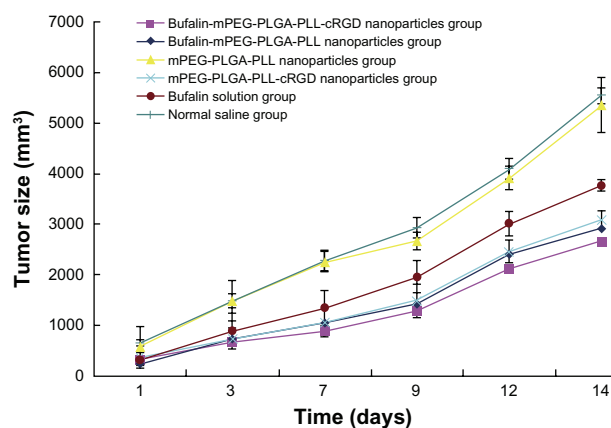
Figure 7 Tumor size in different groups (mm³; n = 10).

longer. This finding suggests that the inclusion of the cRGD moiety resulted in better tumor targeting and longer residue time in vivo. Compared with the in vitro cell experiments, the cRGD showed an efficient targeting property because of nascent vessels in the tumor. We infer that the mPEG-PLGA-PLL-cRGD NPs were targeting tumor tissue and then endocytosis resulted in uptake by the tumor cell.

Therapeutic efficacy in colon cancer-bearing mice

After administration we measured the tumor volume at predetermined intervals and calculated the inhibitory rate. As illustrated in Figure 7, compared to the NS treatment, mPEG-PLGA-PLL NP treatment had no effect on the tumor in mice ($P > 0.05$). When the same dose of drug was administered to the mice, the inhibition of tumor was better in the bufalin-mPEG-PLGA-PLL NP group and bufalin-mPEG-PLGA-PLL-cRGD NP group than in the bufalin solution group. The tumor size was significantly smaller in the bufalin-mPEG-PLGA-PLL-cRGD NP group than in the other groups. This indicates the treatment efficiency on colon cancer-bearing mice is significantly enhanced via bufalin-loaded NPs compared to that of a bufalin water solution. This treatment is further improved through cRGD targeting.

Conclusion

In this study, bufalin-mPEG-PLGA-PLL-cRGD NPs in the desired size range for targeting colon cancer were successfully prepared using an emulsion-solvent evaporation method. Our experimental results showed that the bufalin-mPEG-PLGA-PLL-cRGD NPs have a particle size of about 164 nm and an encapsulation efficiency > 80%; these NPs showed an initial burst, which was followed by a sustained

release over 192 hours in vitro. Cytotoxicity of the bufalin-mPEG-PLGA-PLL-cRGD NPs was greater than that of bufalin alone and the bufalin-mPEG-PLGA-PLL NPs. The NPs could be effectively internalized in SW620 colon cancer cells. The targeting property of the cRGD moiety was proven by cell uptake and an in vivo target study. These results implied that the mPEG-PLGA-PLL-cRGD NPs have the ability to enhance the in vivo therapeutic efficacy. However, further experiments should be performed to determine the mechanism underlying this ability of NPs.

Acknowledgments

Disclosure

The authors report no conflicts of interest in this work.

References

1. Henley SJ, King JB, German RR, et al. Surveillance of screening-detected cancers (colon and rectum, breast, and cervix) – United States, 2004–2006. *MMWR Surveill Summ*. 2010;59(9):1–25.
2. Sjo OH, Berg M, Merok MA, et al. Peritoneal carcinomatosis of colon cancer origin: highest incidence in women and in patients with right-sided tumors. *J Surg Oncol*. 2011;104(7):792–797.
3. Lu CX, Nan KJ, Lei Y. Agents from amphibians with anticancer properties. *Anticancer Drugs*. 2008;19(10):931–939.
4. Cui X, Inagaki Y, Xu H, et al. Anti-hepatitis B virus activities of cinobufacini and its active components bufalin and cinobufagin in HepG2.2.15 cells. *Biol Pharm Bull*. 2010;33(10):1728–1732.
5. Qi F, Li A, Inagaki Y, et al. Antitumor activity of extracts and compounds from the skin of the toad Bufo bufo gargarizans Cantor. *Int Immunopharmacol*. 2011;11(3):342–349.
6. Han KQ, Huang G, Gu W, et al. Anti-tumor activities and apoptosis-regulated mechanisms of bufalin on the orthotopic transplantation tumor model of human hepatocellular carcinoma in nude mice. *World J Gastroenterol*. 2007;13(24):3374–3379.
7. Li H, Wang P, Gao Y, et al. Na+/K+-ATPase alpha3 mediates sensitivity of hepatocellular carcinoma cells to bufalin. *Oncol Rep*. 2011;25(3): 825–830.
8. Amano Y, Cho Y, Matsunawa M, et al. Increased nuclear expression and transactivation of vitamin D receptor by the cardiotonic steroid bufalin in human myeloid leukemia cells. *J Steroid Biochem Mol Biol*. 2009;114(3–5):144–151.
9. Zhu Z, Yu Y, Wang K, et al. Effect of Bufalin on proliferation and apoptosis of human non-small cell lung cancer A549 cell. *Zhongguo Fei Ai Za Zhi*. 2010;13(9):841–845.
10. Li D, Qu X, Hou K, et al. PI3 K/Akt is involved in bufalin-induced apoptosis in gastric cancer cells. *Anticancer Drugs*. 2009;20(1):59–64.

11. Yu CH, Kan SF, Pu HF, et al. Apoptotic signaling in bufalin- and cinobufagin-treated androgen-dependent and -independent human prostate cancer cells. *Cancer Sci*. 2008;99(12):2467–2476.

12. Gong LL, Li JX, Zhang HM. Progress on pharmacological action and preparation of venenum bufonis. *Food and Drug*. 2007;9(10):51–53.

13. Xu YZ, Fan Y, Zhang YL, et al. Effects of bufalin on apoptosis of human colon cancer SW620 cell. *J Jiangsu University (Medicine Edition)*. 2007;17(6):515–517.

14. Xie CM, Chan WY, Yu S, et al. Bufalin induces autophagy-mediated cell death in human colon cancer cells through reactive oxygen species generation and JNK activation. *Free Radic Biol Med*. 2011;51(7):1365–1375.

15. Bick RJ, Poindexter BJ, Sweney RR, et al. Effects of Chan Su, a traditional Chinese medicine, on the calcium transients of isolated cardiomyocytes: cardiotoxicity due to more than Na, K-ATPase blocking. *Life Sci*. 2002;72(6):699–709.

16. Liu PF, Zhu MJ, Li YG, Wang HZ, Duan YR. The research on cytotoxicity and cellular uptake of mPEG-PLGA-PLL nanoparticles. Proceedings of 2009 international conference on advanced fibers and polymer materials. 2009;1–2:1190–1192.

17. Kostakis C, Byard RW. Sudden death associated with intravenous injection of toad extract. *Forensic Sci Int*. 2009;188(1–3):e1–e5.

18. Dasgupta A, Emerson L. Neutralization of cardiac toxins oleandrin, oleandrigenin, bufalin, and cinobufotalin by digibind: monitoring the effect by measuring free digitoxin concentrations. *Life Sci*. 1998;63(9):781–788.

19. Zhu D, Lu X, Hardy PA, et al. Nanotemplate-engineered nanoparticles containing gadolinium for magnetic resonance imaging of tumors. *Invest Radiol*. 2008;43(2):129–140.

20. Hu K, Zhu L, Liang H, et al. Improved antitumor efficacy and reduced toxicity of liposomes containing bufadienolides. *Arch Pharm Res*. 2011;34(9):1487–1494.

21. Weng Y, Jin J, Pan C, et al. Bioavailability and pharmacokinetics of bufadienolides-loaded lipid microspheres after different administrations to rats. *J Lipid Sci Tech*. 2011;113(9):1095–1105.

22. Li F, Wang Y, Liu Z, et al. Formulation and characterization of bufadienolides-loaded nanostructured lipid carriers. *Drug Dev Ind Pharm*. 2010;36(5):508–517.

23. Brigger I, Dubernet C, Couvreur P. Nanoparticles in cancer therapy and diagnosis. *Adv Drug Deliv Rev*. 2002;54(5):631–651.

24. Cegnar M, Kristl J, Kos J. Nanoscale polymer carriers to deliver chemotherapeutic agents to tumours. *Expert Opin Biol Ther*. 2005;5(12):1557–1569.

25. Murphy EA, Majeti BK, Barnes LA, et al. Nanoparticle-mediated drug delivery to tumor vasculature suppresses metastasis. *Proc Natl Acad Sci U S A*. 2008;105(27):9343–9348.

26. Ryppa C, Mann-Steinberg H, Biniossek ML, et al. In vitro and in vivo evaluation of a paclitaxel conjugate with the divalent peptide E-[c(RGDfK)2] that targets integrin alpha v beta 3. *Int J Pharm*. 2009;368(1–2):89–97.

27. Stupack DG, Puente XS, Boutsaboualoy S, et al. Apoptosis of adherent cells by recruitment of caspase-8 to unligated integrins. *J Cell Biol*. 2001;155(3):459–470.

28. Burkhart DJ, Kalet BT, Coleman MP, et al. Doxorubicin-formaldehyde conjugates targeting alphavbeta3 integrin. *Mol Cancer Ther*. 2004;3(12):1593–1604.

29. Zange R, Li YX, Kissel T. Biocompatibility testing of ABA triblock copolymers consisting of poly(L-lactic-co-glycolic acid) A blocks attached to a central poly(ethylene oxide) B block under in vitro conditions using different L929 mouse fibroblasts cell culture models. *J Control Release*. 1998;56(1–3):249–258.

30. Sawhney AS, Pathak CP, Hubbell JA. Interfacial photopolymerization of poly(ethylene glycol)-based Anderson JM, Shive. Biodegradation and biocompatibility of PLA and PLGA microspheres. *Adv Drug Delivery Rev*. 1997;28(1):5–24.

31. Jain R, Shah NH, Malick AW, Rhodes CT. Controlled drug delivery by biodegradable poly(ester) devices: Different preparative approaches. *Drug Dev Res*. 1998;24(8):703–727.

32. Hudecz F, Kutassikovacs S, Mezo G, Szekerke M. Biodegradability of synthetic branched polypeptide with poly(l-lysine) backbone *Biol. Chem Hoppe-Seyler*. 1989;370(9):1019–1026.

33. Sawhney AS, Pathak CP, Hubbell JA. Interfacial photopolymerization of poly(ethylene glycol)-based hydrogels upon alginate-poly(l-lysine) microcapsules for enhanced biocompatibility. *Biomaterial*. 1993;14(13):1008–1016.

34. Akizawa T, Kino K, Kinugasa E, et al. Clinical effects of a polyethylene glycol grafted cellulose membrane on thrombogenicity and biocompatibility during hemodialysis. ASAIO transactions/American Society for Artificial Internal Organs. 1990;36(3):M640–M642.

35. Maeda H, Wu J, Sawa T, Matsumura Y, Hori K. Tumor vascular permeability and the EPR effect in macromolecular therapeutics: a review. *J Control Release*. 2000;65(1–2):271–284.

36. Li Q, Wang Y, Feng N, Fan Z, Sun J, Nan Y. Novel polymeric nanoparticles containing tanshinone IIA for the treatment of hepatoma. *J Drug Target*. 2008;16(10):725–732.

37. Liu D, Feng JF. Determination of apparent aqueous solubility and apparent oil-water partition coefficients of three bufadienolides composition. *Zhongguo Zhong Yao Za Zhi*. 2008;33(11):1256–1258.

38. Pan G, Lemmouchi Y, Akala EO, et al. Studies on PEGylated and drug-loaded PAMAM dendrimers. *J Bioact Compat Pol*. 2005;20(1):113–128.